Accretion and Jet Coupling in Powerful Radio Quasars at Cosmic Noon

MOJEGAN AZADI,¹ BELINDA WILKES,¹ JOANNA KURASZKIEWICZ,¹ S. P. WILLNER,¹ AND MATTHEW L. N. ASHBY¹

¹ Center for Astrophysics | Harvard & Smithsonian, 60 Garden Street, Cambridge, MA, 02138, USA

ABSTRACT

We present bolometric corrections, as a function of wavelength, for powerful radio-loud quasars from the Revised Third Cambridge Catalogue of Radio Galaxies (3CRR) at 1 < z < 2. The bolometric luminosities are derived by integrating the intrinsic accretion disk spectral energy distributions (SEDs) over the range $1 \,\mu\text{m}$ – $10 \,\text{keV}$ (excluding reprocessed infrared emission) and integrating over inclination angles (to account for accretion disk emission anisotropy). We use accretion disk models, fitted to observed data, to self-consistently bridge the unobserved wavelength region between the UV and Xrays with no need for far-UV gap repair. The resulting bolometric corrections span a wide range $(\sim 1-400)$ across different wavelengths, showing minimal dependence on redshift, X-ray luminosity, and black hole mass, which is possibly due to a narrow range of these intrinsic AGN parameters in the sample. However, when the sample is divided by Eddington ratio, the X-ray bolometric corrections exhibit distinctly different values, with higher correction factors corresponding to higher Eddington ratios. We also examine the connection between total radio luminosity and accretion disk power. For most 3CRR sources, the radio power constitutes roughly 1%-10% of the accretion disk luminosity. However, quasars with compact jets exhibit higher radio luminosities for a given accretion disk power. This suggests a higher efficiency of conversion of accretion power to radio luminosity in the younger jets. Our results provide physically motivated bolometric corrections for powerful radio quasars that are applicable to powerful radio-loud quasars at any epoch.

Keywords: Quasars: Radio-Loud – AGN: high-redshift – SED: galaxies – galaxies: active – AGN: Bolometric correction

1. INTRODUCTION

Active Galactic Nuclei (AGN) release immense energy as they accrete matter, producing radiation that spans the full electromagnetic spectrum. Quantifying this total radiative output—the bolometric luminosity—is crucial for tracing the growth of supermassive black holes (SMBHs) and their impact on galaxies. Ideally, the bolometric luminosity would be measured by integrating the AGN's spectral energy distribution (SED) over all wavelengths, yet observational coverage is typically incomplete. Therefore, empirical bolometric corrections are used instead to infer the total luminosity from observations within limited spectral ranges.

The definition of what constitutes the total radiative output of an AGN remains an open issue (for a full discussion, see Azadi et al. 2025). Some studies define the bolometric luminosity as arising solely from the intrinsic emission of the accretion disk, typically integrating from the optical to the X-ray regime (e.g., Marconi et al. 2004; Nemmen & Brotherton 2010; Runnoe et al. 2012;

Azadi et al. 2025), while others also include the infrared contribution from dust heated by the central source (e.g., Elvis et al. 1994; Richards et al. 2006). The distinction reflects whether the reprocessed mid-infrared emission is considered part of the primary energy budget or a secondary manifestation of the same photons. In addition, anisotropy in the disk emission and relativistic effects—such as Doppler boosting, aberration, and light bending—impose a strong dependence on inclination angle, making it challenging to use uniform bolometric corrections for individual AGN. (e.g., Hubeny et al. 2001; Nemmen & Brotherton 2010).

A central question is which wavelength band provides the most reliable proxy for bolometric luminosity, and which physical parameters—such as AGN luminosity, black hole mass, Eddington ratio, and/or spin—primarily govern it (e.g., Marconi et al. 2004; Vasudevan & Fabian 2007; Hopkins et al. 2007; Netzer 2019; Azadi et al. 2025). In a recent study, Azadi et al. (2025) investigated these questions by constructing a comprehensive grid of accretion-disk SEDs using the

AZADI ET AL.

QSOSED model (Kubota & Done 2018). The integration was carried out over $1 \mu \text{m}$ -10 keV, encompassing emission from the accretion disk and corona as the primary radiative components while explicitly excluding reprocessed infrared radiation from the dusty torus. From this model grid, bolometric corrections were derived as a function of SMBH mass (M_{SMBH}) , Eddington ratio ($\lambda_{\rm Edd}$), spin($a \equiv cJ/GM_{\rm SMBH}^2$), and inclination (θ) . The analysis provides a unified physical framework linking the intrinsic properties of the central engine to the observed luminosities and includes direct comparisons with earlier empirical and theoretical prescriptions. Azadi et al. (2025) show that the bolometric output of an AGN is primarily determined by the accretion rate and SMBH mass, with smaller but noticeable effects from spin and inclination. Increasing SMBH mass produces cooler accretion disks with SEDs peaking at longer wavelengths, whereas higher Eddington ratios or larger spins yield hotter disks which SEDs peak in the far-UV. Inclination further modifies the observed SED, reducing the optical-UV emission (when inclination increases) while leaving the X-ray flux nearly isotropic. As a result, bolometric corrections in the optical-near-UV range ($\sim 5100-3000\,\text{Å}$) are most sensitive to SMBH mass, whereas X-ray corrections depend more strongly on the Eddington ratio. Near the SED peak in the far-UV ($\sim 1450 \,\text{Å}$), these dependencies weaken, making this band a particularly robust and physically motivated reference for estimating bolometric luminosities (see also Azadi et al. 2025).

In this study, we apply the framework for deriving bolometric corrections based on accretion disk and corona emission developed by Azadi et al. (2025) to a sample of 20 radio-loud quasars at 1 < z < 2, drawn from the Revised Third Cambridge Catalogue of Radio Galaxies (3CRR; Laing et al. 1983), in order to determine their intrinsic radiative power. The full multiwavelength SEDs, spanning from radio to X-rays, and their detailed fits for this quasar sample were presented in Azadi et al. (2023). We apply the bolometric correction methodology of Azadi et al. (2025) to the best-fit accretion disk models from Azadi et al. (2023) to determine the bolometric luminosities and bolometric correction factors for the sample.

The paper is organized as follows: Section 2 describes the sample and data; Section 3 summarizes the SED modeling presented in Azadi et al. (2023); Section 4 presents the derived bolometric corrections; and Section 5 provides a summary of our results.

In this study, we aim to determine the bolometric correction factors of the most powerful radio-loud quasars at 1 < z < 2. For this purpose, we focus on sources from the Revised Third Cambridge Catalogue of Radio Galaxies (3CRR; Laing et al. 1983). The full 3CRR catalog contains 173 FR II radio galaxies out to z < 2.5 and is 96% complete down to a flux density of 10 Jy at 178 MHz. Within the redshift range 1 < z < 2, the catalog includes 38 broad- and narrow-line radio galaxies (Wilkes et al. 2013), of which 20 are broad-line objects (i.e., quasars) studied in this work (see Table 1).

We constructed radio-to-X-ray SEDs for these 20 quasars by combining new and archival photometry from multi-frequency radio observations, SMA, ALMA, Herschel, WISE, Spitzer, 2MASS, UKIRT, SDSS, XMM-Newton, and Chandra (see Azadi et al. 2023, for details). This provides a complete, randomly-oriented sample with extensive wavelength coverage spanning nearly ten orders of magnitude in frequency. The SEDs were modeled using the state-of-the-art ARXSED framework, as described below.

3. ARXSED MODEL

ARXSED is a semi-empirical framework designed to reproduce the emission from all major AGN components simultaneously, including the radio lobes and jets, the dusty torus, the accretion disk, and the host galaxy. At radio wavelengths, the model accounts for emission from extended lobes, jets, cores, and hot spots using single or double power laws, parabolic functions, or combinations thereof. To capture the observed steepening of synchrotron spectra, ARXSED includes an exponential cutoff at high frequencies.

In the infrared, ARXSED adopts the two-phase torus model of Siebenmorgen et al. (2015), in which dust can reside in a homogeneous disk, a clumpy medium, or a mixture of both. At optical-UV-X-ray wavelengths, it incorporates the accretion-disk model of Kubota & Done (2018), which divides the emission into three regions: (1) an inner hot corona with electron temperatures $kT_e \sim 40\text{--}100\,\mathrm{keV}$ producing hard Comptonization and hard X-rays; (2) an intermediate region with $kT_e \sim 0.1-1\,\mathrm{keV}$ producing soft Comptonization and soft X-rays; and (3) an outer region responsible for the thermal UV-optical continuum. We note that any non-thermal component associated with the radio structure is not included in the X-ray component (see Section 4.3). Host-galaxy emission from radio to UV wavelengths is modeled using the MAGPHYS framework (da Cunha et al. 2008, 2015). For the present sample, ARXSED yields intrinsic SEDs after correcting for red-

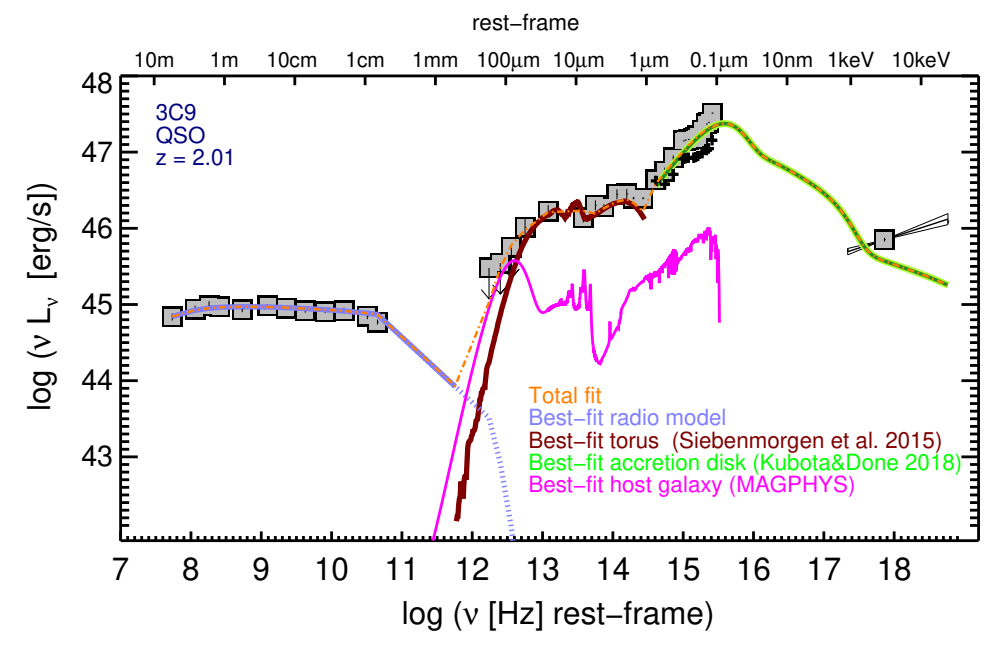


Figure 1. The intrinsic SED of 3C 9 from Azadi et al. (2023). Grey boxes show the photometry, with black plus signs indicating the observed photometric points prior to extinction correction. Colored lines trace the emission components of the best-fit ARXSED model. AGN components include the accretion disk (green), torus (red), and radio emission (light blue). The radio component (light blue) encompasses the lobes, and the dotted extension shows the synchrotron cutoff due to aging electron populations. The host galaxy contribution is shown in magenta.

Table 1. 3CRR quasars: redshift, intrinsic X-ray luminosity (0.3–8 keV), black-hole mass, Eddington ratio, and bolometric luminosity.

Source	z	$\log L_{0.3-8 \mathrm{keV}}^{(1)} \ (\mathrm{erg \ s^{-1}})$	$M_{\rm BH}^{(2)} \ (10^9 M_{\odot})$	$\log \lambda_{ m Edd}^{(3)}$	$L_{\rm bol}~({\rm erg~s^{-1}})$
3C009	2.009	45.85	3.8	-0.4	2.36×10^{47}
3C014	1.469	45.97	9.6	-0.4	5.25×10^{47}
3C043	1.459	45.77	2.1	-1.0	5.25×10^{46}
3C181	1.382	45.71	1.7	-0.6	6.71×10^{46}
3C186	1.067	45.35	1.5	-0.6	5.98×10^{46}
3C190	1.195	45.54	6.0	-1.0	1.04×10^{47}
3C191	1.956	45.86	1.8	-0.6	7.52×10^{46}
3C204	1.112	45.86	2.9	-1.0	5.58×10^{46}
3C205	1.534	46.11	9.8	-0.8	2.70×10^{47}
3C208	1.110	45.65	1.5	-0.4	1.06×10^{47}
3C212	1.048	46.00	6.0	-1.2	7.38×10^{46}
3C245	1.029	45.84	1.1	-0.6	5.33×10^{46}
$3\mathrm{C}268.4$	1.398	45.94	6.2	-1.0	1.04×10^{47}
$3\mathrm{C}270.1$	1.532	45.87	4.6	-1.0	7.01×10^{46}
3C287	1.055	45.57	1.5	-1.2	1.78×10^{46}
3C318	1.574	45.50	2.4	-1.6	1.14×10^{46}
3C325	1.135	45.22	3.8	-1.4	2.02×10^{46}
$4\mathrm{C}16.49$	1.880	46.03	2.1	-1.4	1.61×10^{46}
3C432	1.785	45.79	4.7	-1.2	1.78×10^{46}
3C454.0	1.757	45.70	0.8	0.0	1.32×10^{47}

Notes. (1) $L_{\rm X}$ values are from Wilkes et al. (2013). (2) $M_{\rm BH}$ values are from Azadi et al. (2023). (3) Eddington ratios ($\lambda_{\rm Edd}$) are from Azadi et al. (2023).

4 Azadı et al.

dening and absorption in the torus, the host galaxy, and the Milky Way.

The modeling proceeds as follows. First, ARXSED corrects the photometry between 0.91 and $13 \,\mu\mathrm{m}$ for Galactic absorption using the attenuation law $\tau_{\lambda} \propto$ $\lambda^{-0.7}$ from Charlot & Fall (2000). It then fits the torus emission and corrects the optical-UV photometry for internal obscuration (see Equation 16 in Azadi et al. 2023; Siebenmorgen et al. 2015). X-ray luminosities are assumed to be intrinsic, corrected for both Galactic and intrinsic absorption (Wilkes et al. 2013; Azadi et al. 2023). To model the optical-UV-X-ray portion of the SED, Azadi et al. (2023) employed the Kubota & Done (2018) accretion-disk model, generating $\sim 11,000$ templates spanning a large range of the main physical parameters: SMBH mass, Eddington ratio, spin, and viewing angle. Where available, emission-line features (e.g., Mg II and C IV FWHM) were used as priors for SMBH mass, and templates were built accordingly. For sources without such spectroscopic information, the average values from those with prior mass estimates were used. However, this mass was used only as an initial estimate, allowing $M_{\rm BH}$ of the templates to vary within $\pm 1 {\rm dex}$ of that value. The viewing angle of each accretiondisk template was restricted to within $\pm 12^{\circ}$ of the bestfit torus orientation, yielding a median inclination of $52^{\circ} \pm 5^{\circ}$ for this quasar sample.

The best-fit radio-to-X-ray SEDs for the 20 quasars in our sample, along with estimates of the physical properties of the central engine (SMBH mass, Eddington ratio, spin), the torus (viewing angle, dust filling factor, optical depth), and the host galaxy (stellar mass, star formation rate), are presented in Azadi et al. (2023). As an example, Figure 1 shows the radio-to-X-ray SED and corresponding ARXSED fit for the quasar 3C 9.

4. ESTIMATING BOLOMETRIC LUMINOSITY OF 3CRR QUASARS

To estimate the bolometric luminosities, and bolometric correction factors for each of the 3CRR quasars, we used the best-fitting accretion disk models from ARXSED (Azadi et al. 2023). The bolometric luminosity was obtained by integrating the intrinsic (rather than observed) SED from $1\,\mu\mathrm{m}$ to $10\,\mathrm{keV}$, and the bolometric correction factor is defined as

$$BC(\nu, \theta) \equiv \frac{\int_0^{\pi/2} \sin \theta \int_{1 \,\mu \text{m}}^{10 \,\text{keV}} L_{\nu}(\theta) \, d\nu \, d\theta}{\nu L_{\nu}(\theta)}, \qquad (1)$$

for any specified frequency ν and inclination angle θ . Although the ARXSED best fit corresponds to a single inclination angle, we integrate over all θ to fully account for the anisotropy of the accretion disk emis-

sion. Mid-infrared emission from the torus is excluded from the integration because it is dominated by reprocessed accretion-disk radiation already included in the model. The accretion-disk templates (see Figure 1) self-consistently bridge the otherwise unobserved region between the UV and soft X-ray bands, removing the need for empirical gap-repair methods. By integrating over all angles, our approach naturally incorporates the geometric anisotropy of disk radiation, and thus no additional isotropy correction is required. Table 1 lists the bolometric luminosities estimated for the 20 sources in our sample, calculated using Equation 1.

Figure 2 (tabulated in Table 2) shows the bolometric correction as a function of rest-frame frequency for the 3CRR quasars at $1 < z \lesssim 2$. The light purple region indicates the full range of values across the sample, while the dark purple shading marks the interquartile range (25th-75th percentile), and the solid curve represents the sample median. The bolometric correction reaches a minimum near $\log \nu \sim 15.4$, corresponding to a wavelength of $\sim 0.1 \,\mu\text{m}$, where the accretion disk SEDs typically peak. At wavelengths farther from this peak, the bolometric correction increases, although the scatter within the interquartile range remains relatively small and nearly constant. Toward the X-ray regime, the percentile range in Figure 2 broadens, which primarily reflects the strong dependence of the bolometric correction in the X-ray range on the Eddington ratio (see the discussion below and also Azadi et al. 2025). This behavior is intrinsically captured in the QSOSED model, as the accretion disk SEDs at X-rays are constructed to be independent of parameters such as SMBH mass, spin, and inclination. The model assumes an increase in the Eddington ratio leads to an increase in luminosity (Ho 2008) and is accompanied by a systematic steepening of both $\alpha_{\rm ox}$ and the X-ray photon index $\Gamma_{2-10\,{\rm keV}}$ (see Kubota & Done 2018 for a detailed discussion). The interplay of these trends results the bolometric correction in the X-ray band particularly sensitive to variations in the Eddington ratio.

4.1. Bolometric Correction Dependence on Quasars' Properties

Figure 3 shows the bolometric corrections for the 3CRR quasars, divided into two bins based on the average value of each parameter in the sample: redshift, X-ray luminosity, SMBH mass, and Eddington ratio. The intrinsic X-ray luminosities are taken from Wilkes et al. (2013), while the SMBH masses and Eddington ratios are derived from the ARXSED fits (see Table 6 of Azadi et al. 2023). Because of the small sample size and the limited range of parameter values, the envelopes of

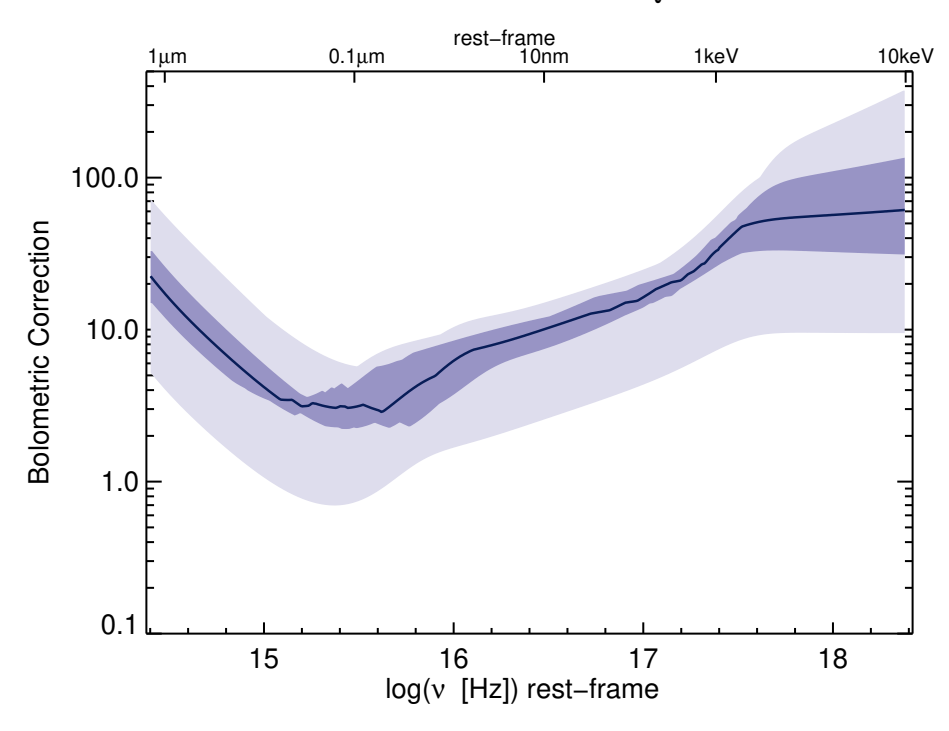


Figure 2. Bolometric correction factor as a function of frequency for the 20 3CRR radio-loud quasars at $z \sim 1$ (Azadi et al. 2023). The solid curve represents the median bolometric correction. The dark purple shading indicates the interquartile (25th–75th percentile) range, while the light purple region shows the full range of values across the sample. Correction factors are derived from the best-fit accretion disk models of Azadi et al. (2023), using the integral defined in Equation 1.

Table 2. The median bolometric correction values (with their corresponding 25th–75th percentile ranges), plotted in Figure 2 as a function of frequency

$\log \nu$ (rest-frame)	Bolometric Correction
14.5	$16.1_{11.2}^{24.3}$
14.7	$7.86^{11.7}_{5.67}$
15.0	$4.17^{5.92}_{3.51}$
15.3	$3.26^{3.68}_{2.56}$
15.5	$3.14_{2.26}^{4.65}$
15.7	$3.77_{2.35}^{6.58}$
16.0	$6.26^{8.48}_{3.75}$
16.3	$8.21_{5.97}^{10.3}$
16.5	$10.3_{7.60}^{12.2}$
16.7	$12.9_{10.0}^{16.4}$
17.0	$16.4_{14.0}^{20.2}$
17.3	$23.6_{20.4}^{28.6}$
17.5	$45.1_{31.0}^{56.0}$
18.0	$56.9^{110.4}_{32.4}$

the bolometric corrections largely overlap at most frequencies, indicating no significant dependence on these quantities.

The redshift panel (top left) shows a broader range for the higher-redshift bin, although the frequency at which the bolometric correction reaches its minimum is nearly identical between the low- and high-redshift subsamples (median curves at $\log \nu \sim 15.4$ for both). Both sub-samples exhibit a wider spread at X-ray frequencies, primarily due to variations in the Eddington ratio, as discussed below.

The top-right panel of Figure 3 shows the sample divided according to X-ray luminosity, where $L_{\rm X}$ is the rest-frame $L_{0.3-8\,{\rm keV}}$ luminosity corrected for any significant intrinsic absorption, $N_{\rm H,int}$. Because all of our sources are quasars, they span only a narrow range in $N_{\rm H,int}$. For sources with low X-ray net counts, $N_{\rm H}$ was not well constrained, and a 3σ upper limit was adopted instead (see Wilkes et al. 2013). In such cases, the intrinsic X-ray luminosity may be slightly overestimated. The bolometric correction reaches its minimum at slightly lower frequencies in the higher- $L_{\rm X}$ bin (log $\nu \sim 15.6$) compared to the lower- $L_{\rm X}$ bin (log $\nu \sim 15.6$). The low- $L_{\rm X}$ subsample exhibits a larger dispersion in bolometric correction, likely because of sources with lower X-ray counts and hence lower $L_{\rm X}$.

The trends with SMBH mass and Eddington ratio reflect how these parameters shape the accretion-disk SED (Azadi et al. 2025). An increase in SMBH mass results in a cooler accretion disk and shifts its SED peak toward lower frequencies, which in turn moves the minimum of the bolometric correction to smaller $\log \nu$. This trend is evident in Figure 3: the bolometric-correction minimum

6 Azadi et al.

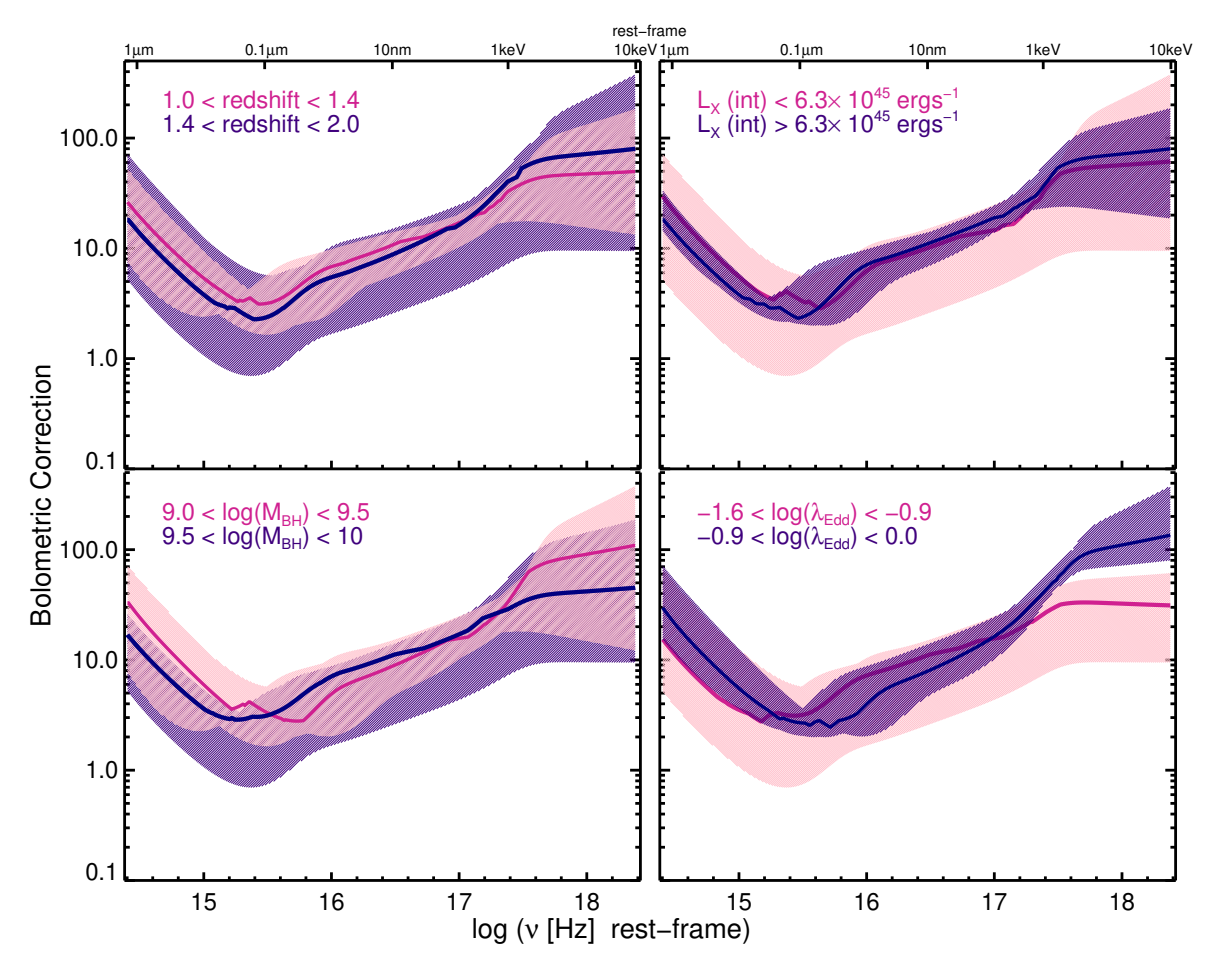


Figure 3. Bolometric correction factor as a function of frequency for the 3CRR quasars at $1 < z \lesssim 2$. Each panel shows the sample divided into two bins based on the average value of a given parameter: redshift, X-ray luminosity, SMBH mass, and Eddington ratio. The intrinsic X-ray luminosities are adopted from Wilkes et al. (2013), while the SMBH masses and Eddington ratios are derived from the ARXSED fits (see Table 6 of Azadi et al. 2023).

occurs at log $\nu \simeq 15.3$ for the higher-mass bin, compared to $\log \nu \simeq 15.7$ for the lower-mass bin. At frequencies below this dip, more massive systems emit a larger fraction of their total luminosity, resulting in smaller bolometric corrections; at higher frequencies, the opposite holds true.

In contrast, variations in the Eddington ratio have the opposite effect. A higher Eddington ratio increases the accretion rate relative to the Eddington limit, producing a hotter disk whose emission peaks at higher frequencies in the far-UV. As a result, the minimum of the bolometric correction shifts toward higher $\log \nu$, occurring at $\log \nu \simeq 15.7$ for the higher- $\lambda_{\rm Edd}$ bin and at $\log \nu \simeq 15.2$ for the lower- $\lambda_{\rm Edd}$ bin. At frequencies above the SED peak, this trend reverses, as hotter disks radiate a larger fraction of their luminosity at higher energies. In the X-ray regime, however, accretion disk models with the same SMBH mass and spin converge to similar νL_{ν} values (see Azadi et al. 2025, for details), resulting in the

Table 3. Bolometric correction values for the 3CRR quasars at five commonly used bands in the literature

Wavelength (rest-frame)	Bolometric Correction		
$5100\mathrm{\AA}$	$7.38^{10.9}_{5.34}$		
$3000\mathrm{\AA}$	$4.32_{3.59}^{6.17}$		
$1450\mathrm{\AA}$	$3.13_{2.32}^{3.86}$		
$2\mathrm{keV}$	$32.5^{40.2}_{25.7}$		
$10\mathrm{keV}$	$61.3_{31.2}^{135.}$		

bolometric correction being insensitive to SMBH mass but increasingly dependent on the Eddington ratio.

4.2. Advantages and Limitations of Determining the Bolometric Correction from Accretion Disk Modeling

Estimating bolometric luminosities from the best-fit accretion disk model in ARXSED has several advantages as we elaborate below.

A persistent challenge in constructing AGN SEDs is the lack of coverage between the far-UV and X-ray regimes as it is inaccessible from ground- and space-based observatories, as discussed in detail by Azadi et al. (2025). Many previous studies have bridged this gap by interpolating in $\log \nu - \log(\nu L_{\nu})$ space (e.g., Elvis et al. 1994; Richards et al. 2006; Runnoe et al. 2012). In contrast, ARXSED models the full SED self-consistently across the radio–to–X-ray range, predicting the spectral shape even in wavelength regions with limited observational data (see Azadi et al. 2023).

The 3CRR quasars are among the most powerful AGN, typically powered by optically thick, geometrically thin accretion disks (e.g., Shakura & Sunyaev 1976; Novikov & Thorne 1973). These disks emit strongly across the visible-to-X-ray range, but their radiation is intrinsically anisotropic. Accurately estimating the total radiative output of such systems therefore requires accounting for inclination angle effects. Previous studies often simplified this problem by assuming a single, representative inclination angle for an entire population (e.g., Runnoe et al. 2012), which can underestimate bolometric luminosities (see discussion in Azadi et al. 2025). In this work, we avoid this approximation: the integration defined in Equation 1 explicitly includes the inclination dependence of the accretion disk emission, thereby incorporating anisotropic effects selfconsistently without any additional correction.

Relativistic effects such as Doppler boosting, aberration, and light bending can substantially distort the observed SED of an AGN, leading to deviations from the expectations of a simple Newtonian disk (e.g., Hubeny et al. 2001; Nemmen & Brotherton 2010). These effects become increasingly important at larger inclination angles, where relativistic aberration and beaming enhance the observed anisotropy of the emission (Azadi et al. 2025). In ARXSED, the accretion disk emission is modeled using the QSOSED framework of Kubota & Done (2018), which assumes that the disk truncates near the region responsible for hard X-ray production and does not include strong relativistic reflection or smearing effects (e.g., Yaqoob et al. 2016; Porquet et al. 2018). Instead, the model incorporates a warm Comptonization component to reproduce the soft X-ray excess, consistent with recent evidence favoring Comptonization over relativistic reflection as the dominant origin of this feature (e.g., Porquet et al. 2018).

The literature remains divided on the wavelength range that should be integrated to derive AGN bolometric luminosities (see Section 1). Some studies argue that integrating only over the optical—to—soft X-ray regime provides the most physically meaningful estimate of the

intrinsic emission (e.g., Nemmen & Brotherton 2010; Runnoe et al. 2012; Azadi et al. 2025), while others include the mid-infrared contribution (e.g., Richards et al. 2006), suggesting that MIR emission, being more isotropic, may better trace the total radiative power. Our approach resolves this ambiguity: ARXSED first models the dusty torus and corrects the optical—UV photometry for obscuration accordingly. Integration over $1\,\mu\text{m}-10\,\text{keV}$ thus captures all primary emission from the accretion disk- the same radiation that powers the reprocessed MIR emission—without double counting.

Another advantage of this approach is that it isolates the radiative power from the accretion disk and corona, excluding X-ray emission associated with radio structures such as jets or compact cores (see SED example in Figure 1). In sources with strong radio cores, empirical bolometric estimates based directly on observed X-ray fluxes may therefore overpredict the intrinsic disk radiative output by including non-coronal emission.

Despite these advantages, one limitation of our estimates is the lack of reliable optical or UV photometry for a few objects (e.g., 3C 325 and 4C 16.49), which leads to larger uncertainties in the accretion disk modeling and less tightly constrained parameters.

Table 3 lists the median bolometric correction values derived for the 3CRR quasars at 1 < z < 2, at bands commonly used in the literature. Our results are consistent with, and fall within the range of, previously reported values (e.g., Elvis et al. 1994; Richards et al. 2006; Runnoe et al. 2012). However, those reference samples are largely mixed and predominantly composed of radio-quiet quasars (for details, see Azadi et al. 2025). In contrast, the values reported here are specifically applicable to the radio-loud population. Furthermore, because the QSOSED model is not explicitly redshift-dependent, these bolometric corrections can be robustly applied to radio-loud AGN across cosmic time.

4.3. The Integrated Power at Radio Frequencies

Our sample of 3CRR quasars at $1 < z \lesssim 2$ represents the most luminous radio sources at this epoch. Because the 3CRR catalog is radio-flux-limited, the sample is biased toward quasars with high radio and accretion disk luminosities. Figure 4 illustrates the relationship between the total radio luminosity and the integrated accretion disk (bolometric) luminosity for these quasars. The radio luminosities were computed from the best-fit radio models, integrated from 10^8 Hz up to the cutoff frequency (see Figure 5, and model parameters in Table 7 of Azadi et al. 2023). This cutoff marks the frequency at which energy losses in the electron population cause a rapid decline in radio emission (e.g., Blandford & Königl

8 Azadi et al.

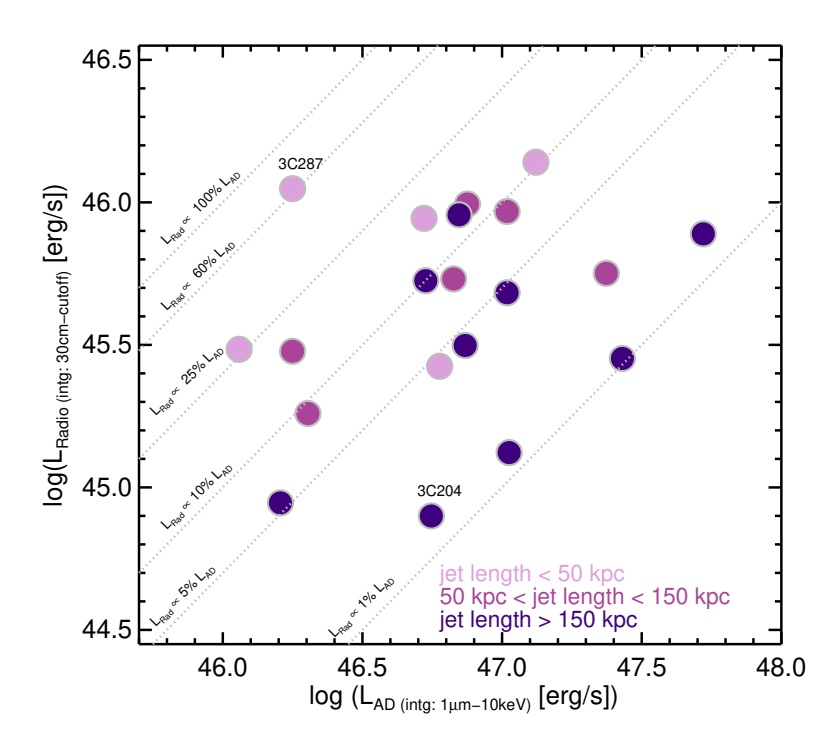


Figure 4. The integrated radio luminosity is plotted against the integrated accretion disk luminosity for quasars hosting young/compact (light purple), intermediate (medium purple), and mature/extended (dark purple) jets. The dotted lines indicate different ratios between the integrated radio and accretion disk luminosities, ranging from 1% to 100%. The SED of the two extreme cases—3C 204 (lowest integrated radio luminosity) and 3C 287 (highest integrated radio luminosity)—are shown in Figure 5.

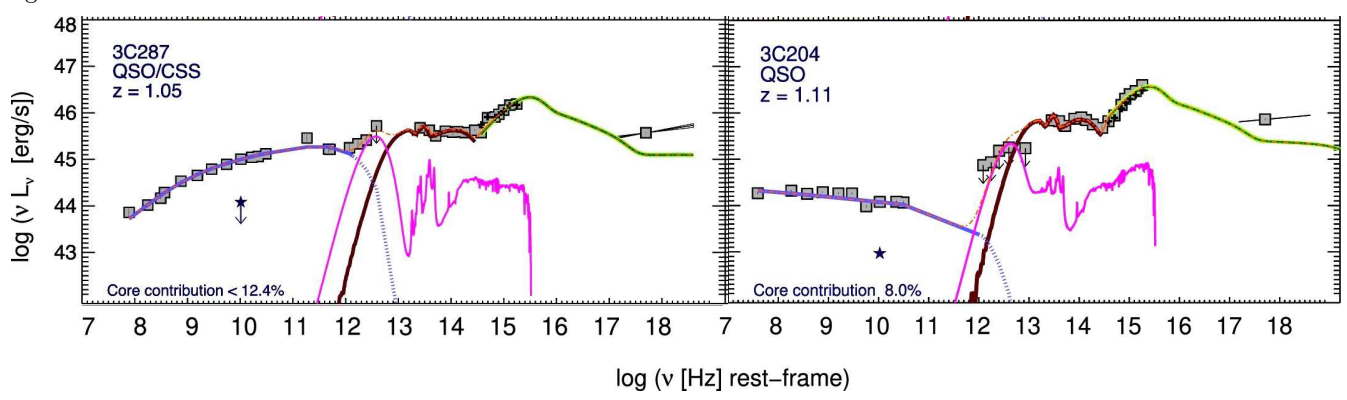


Figure 5. The SED of the two quasars with the highest and lowest integrated radio luminosities, adapted from Azadi et al. (2023). The gray points show the broadband photometry corrected for absorption, while the black plus indicate the visible–UV photometry prior to applying the torus obscuration correction. The colored curves highlight the key emission components: light blue represents the radio emission from the core, jets, hot spots, and lobes (included in the radio integration); dark red corresponds to the infrared radiation from the torus; green traces the thermal emission from the accretion disk extending from the visible to X-ray regime; magenta denotes the stellar emission from the host galaxy; and orange shows the overall combined fit. The dotted light-blue section marks the cutoff frequency where the radio spectrum declines. The dark-blue star indicates the estimated core contribution to the 5 GHz flux density. At X-ray, the black line (or bow tie) represents the power-law model fitted to the absorption-corrected data.

1979; Konigl 1981). In our sample it ranges between 10^{11} and 10^{13} Hz, being higher in quasars with strong core emission (Azadi et al. 2023). The integrated radio luminosities therefore include contributions from all radio components—lobes, jets, cores, and hot spots.

In Figure 4, the sample is divided into three groups based on the de-projected jet length, which also serves as a proxy for jet maturity, with the shortest jets typically representing the youngest systems (Azadi et al. 2023). Figure 4 shows that quasars with smaller jets generally

exhibit higher radio luminosities relative to their accretion disk luminosities than those extremely extended jets (> 150 kpc), suggesting that compact radio quasars may be more efficient at converting accretion power into radio emission, whereas the radio luminosity declines as the jets expand and age. In the majority of the quasars with medium or extended jets, the radio power constitutes approximately 1–10% of the accretion-disk power. The only compact source within this range is 3C 186, whose radio images and SED indicate that it is likely embedded in a dense ISM that hinders the expansion of its radio structure (Azadi et al. 2023). The source with the lowest integrated radio luminosity is 3C 204, whose SED is shown in Figure 5.

Sources above the 10% line tend to have bright cores and/or compact radio jets. This is especially evident for 3C 287, a compact steep-spectrum (CSS) source with an 8 kpc de-projected jet length and a radio SED that remains core-dominated out to infrared wavelengths (see Figure 5 adopted from Azadi et al. 2023).

Figure 5 shows that in our sources an additional non-thermal X-ray component, likely arising from synchrotron self-Compton (SSC) or inverse Compton (IC) processes is required. Such emission may affect both the torus and accretion-disk fits, and consequently the derived luminosities. If this additional X-ray emission were included, the total radiative power of the radio structures would further increase, likely enhancing the observed separation between compact and extended sources. We also note that the integrated radio luminosity combines emission from multiple components—lobes, jets, cores, and hot spots—representing activity over different epochs of an AGN's evolution. In contrast, the accretion disk luminosity traces the current accretion state. Thus, Figure 4 effectively compares radiative power over different timescales. While our findings suggest that compact quasars are brighter radio emitters than their extended counterparts, confirming the nature of this relation will require a larger and more statistically complete sample.

5. SUMMARY

In this study, we applied the methodology developed by Azadi et al. (2025) to a sample of 20 radioloud quasars from the 3CRR catalog at $1 < z \lesssim 2$ (Azadi et al. 2023) for determing their bolometric luminosity. For each source, we determined the bolometric luminosity by integrating the best-fit accretion disk model over the range $1\,\mu\text{m}{-}10\,\text{keV}$ and viewing angles from 0° to 90° . Our main findings are summarized below:

- The bolometric correction factors in the 3CRR quasar sample span a wide range—from ~ 1 to ~ 400 across different wavelengths—although the interquartile range (25th-75th) shows considerably less variation.
- Our bolometric corrections at commonly used wavelengths (5100 Å, 3000 Å, 1450 Å) and X-ray energies (2 keV and 10 keV) are consistent with values reported in the literature, although they exhibit a broader range in the X-ray bands, reflecting the dependence of the X-ray bolometric correction on the Eddington ratio.
- We find no significant dependence of the bolometric correction on redshift, X-ray luminosity, or black hole mass among the 3CRR quasars. Because these quasars occupy a relatively narrow range of intrinsic properties, their overall range of corrections overlaps substantially (Figure 3). However, when the sample is divided by Eddington ratio, the two sub-samples show clearly distinct distributions at X-ray energies—for example, at 10 keV the correction increases from about 30 in the low-Eddington group to roughly 105 in the high-Eddington group, highlighting the dominant impact of Eddington ratio on the X-ray bolometric correction.
- We find no strong correlation between total radio and accretion disk luminosities (Figure 4). For most quasars, the radio power constitutes approximately 1–10% of $L_{\rm AD}$. Nevertheless, the more compact radio sources tend to be brighter in radio emission at a given $L_{\rm AD}$, suggesting that compact radio quasars may be more efficient at converting accretion power into radio luminosity, while the radio output declines as the jets expand and age. Larger samples will be required to confirm these trends with higher statistical significance.

ACKNOWLEDGEMENTS

Support for this work was provided by NASA grants: #80NSSC18K1609, #80NSSC19K1311, #80NSSC20K0043 (MAz), and #80NSSC21K0058 (JK), and by NASA Contract NAS8-03060 *Chandra* X-ray Center (CXC), which is operated by the Smithsonian Astrophysical Observatory (BJW, JK). BJW acknowledges the support of the Royal Society and the Wolfson Foundation. The scientific results in this article are based to a significant degree on observations made by the *Chandra* X-ray Observatory (CXO). This research

10 Azadı et al.

has made use of data obtained from the *Chandra* Data Archive. This research is based on observations made by *Herschel*, which is an ESA space observatory with science instruments provided by European-led Principal Investigator consortia and with important participation from NASA. This work is based in part on observations made with the Spitzer Space Telescope, which was operated by the Jet Propulsion Laboratory, California Institute of Technology under a contract with NASA.

We acknowledge the use of Ned Wright's calculator (Wright 2006) and NASA/IPAC Extragalactic Database (NED), operated by the Jet Propulsion Laboratory, California Institute of Technology, under contract with the National Aeronautics and Space Administration.

The authors would like to thank Chris Done, Małgosia Sobolewska, Mark Birkinshaw and Diana Worrall for helpful comments that improved the quality of the paper.

REFERENCES

Azadi, M., et al. 2023, ApJ, 945, 145

Azadi, M., et al. 2025, arXiv e-prints, arXiv:2509.19666

Blandford, R. D., & Königl, A. 1979, ApJ, 232, 34

Charlot, S., & Fall, S. 2000, ApJ, 539, 718

da Cunha, E., Charlot, S., & Elbaz, D. 2008, MNRAS, 388, 1595

da Cunha, E., et al. 2015, ApJ, 806, 110

Elvis, M., et al. 1994, ApJS, 95, 1

Ho, L. C. 2008, ARA&A, 46, 475

Hopkins, P. F., Richards, G. T., & Hernquist, L. 2007, ApJ, $654,\,731$

Hubeny, I., et al. 2001, ApJ, 559, 680

Konigl, A. 1981, ApJ, 243, 700

Kubota, A., & Done, C. 2018, MNRAS, 480, 1247

Laing, R. A., Riley, J. M., & Longair, M. S. 1983, MNRAS, 204, 151

Marconi, A., et al. 2004, MNRAS, 351, 169

Nemmen, R. S., & Brotherton, M. S. 2010, MNRAS, 408, 1598

Netzer, H. 2019, MNRAS, 488, 5185

Novikov, I. D., & Thorne, K. S. 1973, in Black Holes (Les Astres Occlus), 343–450

Porquet, D., et al. 2018, A&A, 609, A42

Richards, G. T., et al. 2006, ApJS, 166, 470

Runnoe, J. C., Brotherton, M. S., & Shang, Z. 2012, MNRAS, 422, 478

Shakura, N. I., & Sunyaev, R. A. 1976, MNRAS, 175, 613

Siebenmorgen, R., Heymann, F., & Efstathiou, A. 2015, A&A, 583, A120

Vasudevan, R. V., & Fabian, A. C. 2007, MNRAS, 381, 1235

Wilkes, B. J., et al. 2013, ApJ, 773, 15

Wright, E. L. 2006, PASP, 118, 1711

Yaqoob, T., et al. 2016, MNRAS, 462, 4038